

# *panoptica* – instance-wise evaluation of 3D semantic and instance segmentation maps

Florian Kofler<sup>1,2,3,4</sup>, Hendrik Möller<sup>2,4</sup>, Josef A. Buchner<sup>5</sup>, Ezequiel de la Rosa<sup>6,2</sup>, Ivan Ezhov<sup>2,3</sup>,  
Marcel Rosier<sup>2,1</sup>, Isra Mekki<sup>1</sup>, Suprosanna Shit<sup>2</sup>, Moritz Negwer<sup>7</sup>, Rami Al-Maskari<sup>2,7</sup>,  
Ali Ertürk<sup>7,8,9,10</sup>, Shankeeth Vinayahalingam<sup>11,12,13</sup>, Fabian Isensee<sup>14,15</sup>, Sarthak Pati<sup>16,2</sup>,  
Daniel Rueckert<sup>2,17</sup>, Jan S. Kirschke<sup>4</sup>, Stefan K. Ehrlich<sup>18</sup>, Annika Reinke<sup>19</sup>, Bjoern Menze<sup>20</sup>,  
Benedikt Wiestler<sup>4</sup>, and Marie Piraud<sup>1</sup>

<sup>1</sup>Helmholtz AI, Helmholtz Munich, Neuherberg, Germany

<sup>2</sup>Department of Computer Science, TUM School of Computation, Information and Technology, Technical University of Munich, Munich, Germany

<sup>3</sup>TranslaTUM - Central Institute for Translational Cancer Research, Technical University of Munich, Munich, Germany

<sup>4</sup>Department of Diagnostic and Interventional Neuroradiology, School of Medicine, Klinikum rechts der Isar, Technical University of Munich, Munich, Germany

<sup>5</sup>Department of Radiation Oncology, School of Medicine, Klinikum rechts der Isar, Technical University of Munich, Munich, Germany

<sup>6</sup>icomatrix, Leuven, Belgium

<sup>7</sup>Institute for Tissue Engineering & Regenerative Medicine (iTERM), Helmholtz Munich, Neuherberg, Germany

<sup>8</sup>Institute for Stroke and dementia research (ISD), University Hospital, LMU Munich, Munich, Germany

<sup>9</sup>Graduate school of neuroscience (GSN), Munich, Germany

<sup>10</sup>Munich cluster for systems neurology (Synergy), Munich, Germany

<sup>11</sup>Department of Oral and Maxillofacial Surgery, Radboud University Medical Center Nijmegen, Nijmegen, The Netherlands

<sup>12</sup>Department of Artificial Intelligence, Radboud University Medical Center Nijmegen, Nijmegen, The Netherlands

<sup>13</sup>Department of Oral and Maxillofacial Surgery, University Hospital Münster, Münster, Germany

<sup>14</sup>Applied Computer Vision Lab, Helmholtz Imaging, Hamburg, Germany

<sup>15</sup>Division of Medical Image Computing, German Cancer Research Center (DKFZ), Heidelberg, Germany

<sup>16</sup>Department of Pathology and Laboratory Medicine, Indiana University School of Medicine, Indianapolis, USA

<sup>17</sup>Imperial College London, London, United Kingdom

<sup>18</sup>Healthcare Technologies, SETLabs Research GmbH, Munich, Germany

<sup>19</sup>Intelligent Medical Systems (IMS) and HI Helmholtz Imaging, German Cancer Research Center (DKFZ), Heidelberg University, Heidelberg, Germany

<sup>20</sup>Department of Quantitative Biomedicine, University of Zurich, Zurich, Switzerland

## Abstract

*This paper introduces panoptica, a versatile and performance-optimized package designed for computing instance-wise segmentation quality metrics from 2D and 3D segmentation maps. panoptica addresses the limitations of existing metrics and provides a modular framework that complements the original IOU-based Panoptic Quality with other metrics, such as the distance metric ASSD. The package is open-source, implemented in Python, and accompanied by comprehensive documentation and tutorials. panoptica employs a three-step metrics computation process to cover diverse use cases. We demonstrate the efficacy of panoptica on various real-world biomedical datasets, where an instance-wise evaluation is instrumental for an accurate representation of the underlying clinical task. Overall, we envision panoptica as a valuable tool facilitating in-depth evaluation of segmentation methods.*

## 1. Introduction

Segmentation is mostly formulated as a task related to either *stuff*, representing all pixels/voxels belonging to a single class with the same label (*Semantic Segmentation (SemS)*) or *things*, labeling each pixel/voxel of a class (e.g., metastatic tumor lesions) with an individual label (*Instance Segmentation (InS)*) [19].

For many biomedical segmentation problems, an instance-wise evaluation focusing on individual lesions is highly relevant and desirable for both scientific research and clinical applications. This significance is evident in the context of multiple sclerosis, an inflammatory disease characterized by a variable number of white matter lesions in the brain. In the prediction of disease activity, a graph neural network leveraging representations from individual lesions has been suggested [30]. From a clinical perspective, the occurrence of a single new inflammatory lesion is crucial in establishing dissemination in time, playing a pivotal role in the diagnosis and ongoing monitoring of multiple sclerosis

patients [37]. Both the scientific modeling of disease activity as well as the clinical monitoring of patients are clearly dependent on accurate lesion-wise *InS*.

Despite the apparent need for reliable instance-wise segmentation, many biomedical segmentation problems are still addressed as *SemS* problems, partly due to the lack of appropriate instance labels and partly due to the advances in semantic segmentation methodology:

The biomedical image analysis community has successfully developed a plethora of (mostly *U-Net*-based [14, 32]) methods for solving the problem of *SemS* across a range of imaging modalities in diverse applications such as primary brain tumors [2, 20, 21], brain metastases [5, 6], vascular lesions [36], multiple sclerosis [22] or stroke [13] in brain MRI, liver tumors [4, 22] or the spine [33] in CT or light-sheet microscopy tasks [3, 18].

In view of the need for reliable instance-wise segmentation outlined above, there have been attempts to optimize instance awareness in *SemS*, e.g., [22]. Reuniting *stuff* and *things* by simultaneously evaluating *SemS* and *InS* is, therefore, a relevant but unmet need, especially in biomedical image analysis.

**Contribution:** We introduce *panoptica*, a modular, performance-optimized package to compute instance-wise segmentation quality metrics for 2D and 3D semantic- and instance segmentation maps. On an instance level, *panoptica* allows reporting detection metrics, such as *Recognition Quality (RQ)* (equivalent to *F1-score*), and segmentation quality metrics, such as *Segmentation Quality (SQ)* and *Panoptic Quality (PQ)*. Furthermore, additional metrics such as *Average Symmetric Surface Distance (ASSD)* are available. *panoptica* is an open-source Python package, and comprehensive documentation and tutorials are available (cf. Section 3).

To overcome limitations in the PQ metric, which may obscure information related to either detection or segmentation quality [26, 31], *panoptica* focuses on presenting all aspects relevant to instance segmentation tasks by complementing PQ with other pertinent performance metrics.

The metric computation process in *panoptica* is divided into three steps, offering flexibility for various use cases, cf. Sections 3 and 4. In contrast to existing solutions, *panoptica* facilitates the evaluation of semantic segmentation methods at an instance level. We showcase the capabilities of *panoptica* across multiple biomedical data sets featuring real-world segmentation challenges. For these experiments, instance-wise evaluation proves crucial in capturing the nuances of the underlying biomedical tasks. The instance-wise analysis reveals aspects of segmentation quality that may remain concealed when solely evaluating the entire image domain, cf. Section 4.

## 2. Related Work

Kirillov et al. [19] introduce the task of *Panoptic Segmentation (PanS)* as combination of *Semantic Segmentation (SemS)* and *Instance Segmentation (InS)*. They define a *PanS* task as both assigning each pixel to a *class-ID* and an *instance ID*, for *SemS* and *InS* respectively. Further, they propose the *Panoptic Quality (PQ)* metric, cf. Section 3.3. Although the metric was originally proposed for *PanS* tasks, the *Metrics Reloaded initiative* [26] recommended employing the metric also for *InS* tasks. In this context, PQ allows capturing both detection and segmentation quality in one score and is an alternative to the  $F\beta$ -score assessing per-class detection quality.

The PQ metric is implemented as part of the *Medical Open Network for Artificial Intelligence (MONAI) framework* [7] and *torchmetrics* [10]. However, these implementations only support 2D and not 3D input data, and the *torchmetrics* implementation provides no means for instance matching. Therefore, it is only applicable to already matched instance maps. Further, the *Metrics Reloaded initiative* [26] provides a 3D implementation in a *side package* of *MONAI*. While the program can compute PQ, SQ, and RQ, it is designed to always return a single metric. Hence, multiple calls are necessary if all three metrics are required. This is a conscious design choice as the program assumes that the user selects the most suitable metrics via the *Metrics Reloaded framework* [26]. Naturally, the computational overhead of multiple calls leads to a massive accumulation of processing times, prohibiting the evaluation of large-scale data sets. Further, even though computed internally, the package offers no means to return *True Positive (TP)*, *False Positive (FP)*, *False Negatives (FN)*. Unlike *panoptica*, the implementation of the *Metrics Reloaded initiative*, lacking instance approximation capabilities, cannot calculate instance-wise metrics for semantic inputs.

Jungo et al. [17] implement a multitude of segmentation quality metrics in *pymia* [17]; however, the package operates only on whole images and offers no means, for instance, approximation or matching.

Chen et al. [9] provide a good overview of *InS* metrics and introduce a new metric called *SortedAP*, which strictly decreases with both object- and pixel-level imperfections.

### 3. Methods

*panoptica* supports computing instance-wise segmentation, and object detection metrics from *semantic-*, as well as *unmatched* and *matched* segmentation maps, cf. Figure 1.

*panoptica* separates the metric computation process into three steps. This allows building modular metric computation pipelines, as illustrated in Figure 1. Due to its modular software architecture, resembling this three-step process, *panoptica* can easily be extended with additional algorithms for instance approximation, - matching, and metrics. To this end, a framework that automatically validates each input and output and defines all datatypes to be used is established. Therefore, a user extending *panoptica* with a custom algorithm receives immediate and understandable feedback regarding framework fit.

*panoptica* is an open-source package written in Python and included in the [BrainLes](#) project. It can be directly installed from [PyPI](#), and the source code is available on [GitHub](#). Further, *panoptica* is designed to process large-scale data-sets. To achieve fast computation times, it implements parallel computations by leveraging *Python*'s native [multiprocessing](#) library. Additionally, as many segmentation tasks only contain small foreground areas in an otherwise large image, inputs are cropped down to the combined bounding box of both prediction and reference to speed up computations. Detailed performance reports are available in the Supplemental Material, cf. Section 42.2.

The [BrainLes](#) project features several [Jupyter notebook tutorials](#) to illustrate the different use cases for *panoptica* with instance- and semantic segmentation maps. Further, Supplemental Material Section 42.3 illustrates how similarity metric curves can be analyzed in dependency of *Intersection over Union (IOU)* thresholds.

#### 3.1. Instance approximation

While instance-wise metrics can directly be calculated from instance segmentation maps, semantic segmentation maps, by nature, do not contain instance information. Therefore, at the time of release, the *instance approximator* module provides means to approximate instances via *Connected Component Analysis (CCA)*. For this *CCA* users can select between [cc3d](#) [35] and [scipy](#) backends. For most hardware configurations, *cc3d* is expected to perform better on 3D images, while *scipy* promises better 2D performance. Therefore, without user input, *panoptica* defaults to the respective backend for 2D and 3D inputs. For a detailed benchmark of *CCA* backends, cf. Supplemental Material Section 3.1.

#### 3.2. Instance matching

The *instance matcher* module offers means to match instances based on a specified overlap metric. At the time of this writing, we support *IOU* and the *Dice Similarity Coefficient (DSC)*. For simplicity of explanation, we will denote

the selected metric as *Matching Metric (MM)*, its value as *Matching Score (MS)*. The task of the *instance matcher* is to assign each prediction instance to either a reference instance or as *FP*. Each *FP* is relabeled to an unused label so it persists in the map.

We only ever match instances of the prediction to the reference, leaving any given reference map untouched. Depending on the algorithm, we do support many-to-one matching, meaning multiple prediction instances can be matched to the same reference instance.

At the time of release, we offer two distinct instance-matching algorithms. However, the software architecture allows to easily extend *panoptica* with more sophisticated matching algorithms.

##### 3.2.1 Naive Threshold Matcher

The *naive threshold matcher* assigns all prediction instances that exceed a certain user-given *MS* threshold with the reference instance.

If multiple predictions exceed the threshold for the same reference instance, only the one with the highest *MS* is matched to that reference. If the user specified that multiple predictions are allowed to be matched to the same reference instance, each of those matches are kept instead. Should a prediction instance exceed the threshold for multiple reference instances, it is only mapped to the reference instance with the highest *MS*.

##### 3.2.2 Maximize Many-to-One Matcher

This *many-to-one matching* algorithm tries to maximize the *MM* by allowing multiple prediction instances to be assigned to the same reference instance if and only if the combined prediction instances have a greater *MS* than the individual instances. To this end, for each reference instance, it finds the best prediction instance based on the *MM* and then tests for all other instances that have an *MS* greater zero if including it would increase the score. Therefore, this algorithm maximizes the individual specified *MM* when matching but does not provide an overall optimal *MS* solution across all instances.

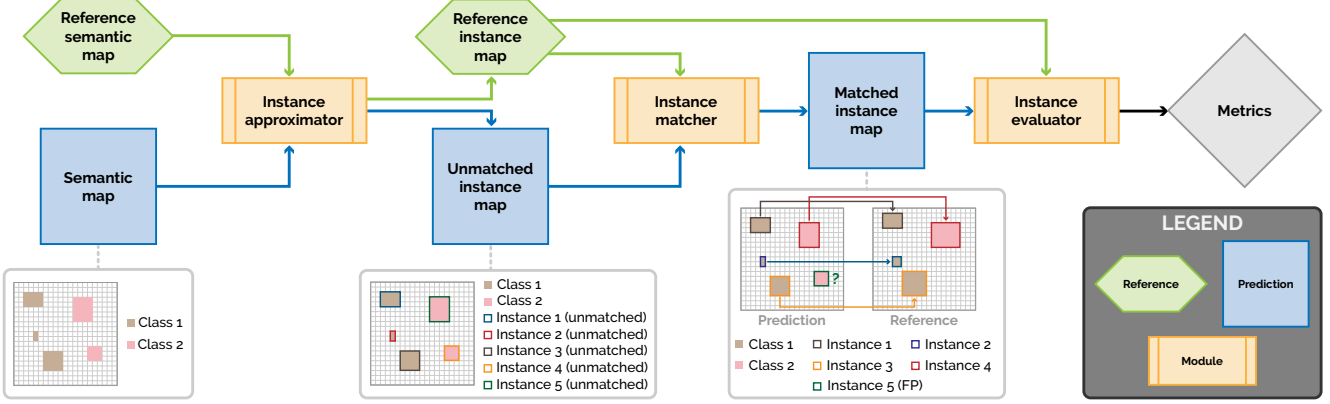


Figure 1. *panoptica*'s modular architecture. Factual *ground truth* is often absent in human-annotated segmentation tasks [23]. Therefore, *panoptica* operates on the concept of comparing *model predictions* to *reference labels*. The first module, *Instance Approximator*, approximates instances; it computes instance maps from both reference and prediction semantic segmentation maps. The second module, *Instance Matcher*, matches an *unmatched instance map* to a *reference instance map*; it outputs a *matched instance map*. The third module, *Evaluator*, computes instance-wise metrics by comparing the *reference instance map* to a *matched instance map*. *panoptica*'s modular architecture allows the assembly of metric evaluation pipelines covering various use cases, cf. Sections 3 and 4.

### 3.3. Instance evaluation

The *instance evaluator* module calculates instance-wise metrics by comparing *reference* to *matched instance* segmentation maps, cf. Figure 1.

Kirillov et al. [19] originally define the Panoptic Quality (PQ) metric as Equations (1) and (2):

$$PQ = \frac{\sum_{(R,P) \in TP} f(R, P)}{|\text{TP}| + 0.5 \cdot |\text{FP}| + 0.5 \cdot |\text{FN}|} \quad (1)$$

$$PQ = \underbrace{\frac{\sum_{(R,P) \in TP} f(R, P)}{|\text{TP}|}}_{\text{Segmentation quality (SQ)}} \cdot \underbrace{\frac{|\text{TP}|}{|\text{TP}| + 0.5 \cdot |\text{FP}| + 0.5 \cdot |\text{FN}|}}_{\text{Recognition quality (RQ)}} \quad (2)$$

where  $R$  refers to the reference instances and  $P$  to the predicted instances, and  $f$  is the similarity metric.

In the original paper Kirillov et al. [19] propose to use *IOU* as similarity metric, while *panoptica* also implements *PQ* based on *DSC* and *ASSD* in addition to *IOU*. Note that the code can easily be modified to integrate further desired metrics, cf. Section 3.

**Edge case handling:** For some edge cases, segmentation metrics are not defined. For example, if both reference and prediction are empty *DSC* and *ASSD* become *NaN*, however, some might argue that *DSC* should be defined as 1.0 for this case. A similar problem occurs for distance-based metrics such as *ASSD*, which become *Inf* if either prediction or reference is empty. *NaN* and *Inf* make it challenging to report aggregated metrics such as the *mean*. Therefore, practitioners developed task-specific mitigation strategies such as assigning a theoretically possible maximum

distance for distance-based metrics [2]. In the absence of a general mitigation strategy producing satisfying results across all use cases, *panoptica* equips users with control over edge case handling.

## 4. Evaluation experiments

We conduct three biomedical evaluation experiments to showcase *panoptica* for various use cases. Across all experiments, we report the *global volumetric Dice Similarity Coefficient (gvDSC)* and the instance-wise *Recognition Quality (RQ)*, *Segmentation Quality (SQ)*, *Panoptic Quality (PQ)* and *Segmentation Quality Average Symmetric Surface Distance (SQASSD)*. Note that *SQASSD* becomes *NaN* for cases with empty prediction and reference, and *Inf* for cases with either empty prediction or empty reference or only unmatched instances, cf. Section 3.3. Therefore, our mean and standard deviation cases are only based on cases that return a number.

### 4.1. VerSe experiment

The *Large Scale Vertebrae Segmentation Challenge (VerSe)* challenge is about localization, labeling, and segmentation of vertebrae in CT scans of arbitrary fields of view [33]. For the segmentation part, the references were *instance maps* with labels that correspond to their anatomical label (i.e., 20 for L1). A simple volumetric *DSC* calculated on a binary version of this mask shows an overall semantic segmentation performance. However, instance-wise metrics are needed to measure how well an algorithm can actually distinguish the different vertebrae. Additionally, as in some cases, the actually different instance labels may be deemed relevant. If a model segments everything correctly but has all labels shifted by one, the resulting overall semantic similarity metric would be terrible, as this is not taken into account. *panoptica* allows the calculation of both metrics dynamically by stating whether the labels of the input maps are assumed to be already matched or not.

**Segmentation Task:** The task in the challenge is that of multi-class instance segmentation, though mainly tackled as a semantic segmentation task by the participants, cf. Figure 2.

**Data:** The dataset features *Computed Tomography (CT)* scans of various scanners, resolutions, and fields of view. We evaluate the segmentation algorithms on the hidden test set of the challenge consisting of 103 subjects. The number of instances can vary between 5 and 25 (mean  $13.08 \pm 5.416$ ) per scan.

**Procedure:** We use the top three submissions from the *VerSe* challenge and evaluate their predictions with the corresponding reference maps. We consider the input to *panoptica* to be unmatched instance maps, as we are not interested in evaluating the labeling capabilities but the segmentation metrics irrespective of their actual predicted vertebra labels. Table 1 illustrates the results of our analysis.

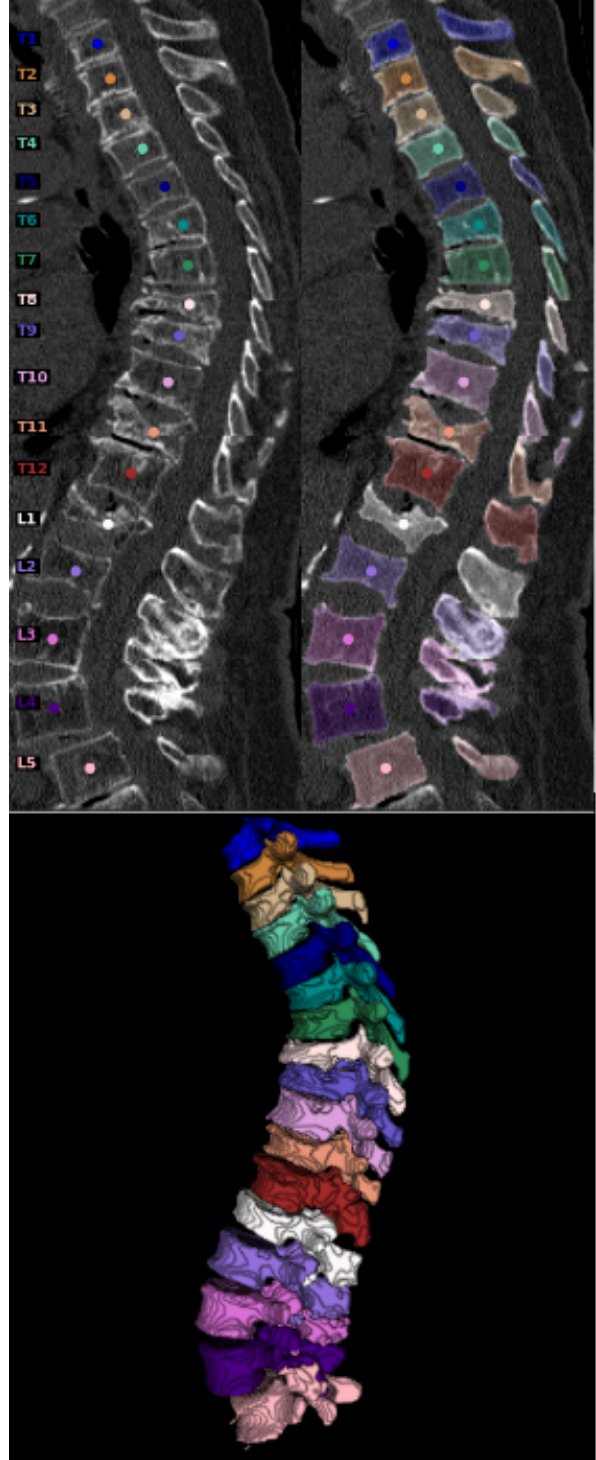


Figure 2. The *VerSe* segmentation challenge task. The reference segmentations for the challenge were generated through a hybrid approach, first being automatically segmented and then manually corrected. This figure shows an exemplary *CT* scan (top-left) of the test set, its reference segmentation mapped on the image (top-right), and a 3D rendering of the reference segmentation (bottom).

Submission	Global Metrics		Instance-wise Metrics		
	$gvDSC \uparrow$	$RQ \uparrow$	$SQ \uparrow$	$PQ \uparrow$	$SQASSD \downarrow$
Payer et al. [29]	$0.932 \pm 0.041$	$0.97 \pm 0.046$	<b><math>0.912 \pm 0.028</math></b>	<b><math>0.886 \pm 0.048</math></b>	<b><math>0.37 \pm 0.055</math></b>
deepreasoningai [8]	<b><math>0.937 \pm 0.036</math></b>	<b><math>0.982 \pm 0.038</math></b>	$0.898 \pm 0.046$	$0.882 \pm 0.063$	$0.414 \pm 0.098$
jdlu [33]	$0.901 \pm 0.037$	$0.947 \pm 0.058$	$0.865 \pm 0.039$	$0.818 \pm 0.059$	$0.601 \pm 0.41$

Table 1. Performance metrics for the top-three submissions of the *VerSe* challenge using an *IOU* threshold of 0.5 for both matching and evaluation. Besides *gvDSC*, we report instance-wise metrics, cf. Section 4. Mean  $\pm$  standard deviation values are reported. Metrics with  $\uparrow$  are better, the higher the value, while  $\downarrow$  is the opposite. The best values for each metric are highlighted in bold. Each algorithm performs quite well. However, although the submission from Chen et al. [8] has the overall best *gvDSC*, it lacks behind Payer. et al. [29] in *SQ*, *PQ*, and *SQASSD*. This suggests the model from Chen et al. [8] is better performing in detecting the correct instances, while the model from Payer. et al. [29] is better at segmenting the instances it correctly detected.

## 4.2. ISLES experiment

The *Ischemic Stroke Lesion Segmentation 2022 challenge (ISLES)* experiment serves as a practical example for the instance-wise evaluation of semantic segmentation maps. The segmentation of ischemia, addressed as a *SemS* task in *Machine Learning (ML)*, is the focus of the ISLES’22 challenge. Despite this, the task and associated data encompass a wide variability of instances (lesions) requiring accurate delineation. Consequently, instance-wise analysis is valuable for tackling the problem. Specifically, the task involves scans featuring multiple non-overlapping embolic brain lesions that exhibit significant variations in terms of size, quantity, and anatomical location.

**Segmentation Task:** The *ISLES* challenge features a binary semantic segmentation task illustrated in Figure 3. The goal is to segment ischemic stroke brain lesions from multi-modal MRI data. Unlike this work, the original challenge evaluates the submissions’ performance using *gvDSC*, *F1-score* as *instance-wise* (here equals lesion-wise) detection, and further clinical metrics such as the differences in absolute lesion volume and absolute lesion count.

**Data:** We analyze the test set of the **ISLES’22 MICCAI challenge** [13]. The dataset consists of 150 multi-center, multi-scanner MR scans. Each exam features three *Magnetic Resonance Imaging (MRI)* sequences, namely *Diffusion Weighted Imaging (DWI)*, *Apparent diffusion coefficient (ADC)*, and *T2-weighted Fluid Attenuated Inversion Recovery (FLAIR)*, accompanied by a label mask encoding the stroke lesions. The data includes a wide variability of image acquisition and stroke patterns. The reference segmentations are obtained through an iterative hybrid algorithm-expert approach and are double-checked by experienced neuroradiologists. The number of non-overlapping instances (i.e., lesions) varies from none (i.e., healthy scans) to a hundred-twenty-six [13].

**Procedure:** In this work, we conduct a complementary analysis to the one conducted in the ISLES’22 challenge by assessing the top-three ranked methods with instance-

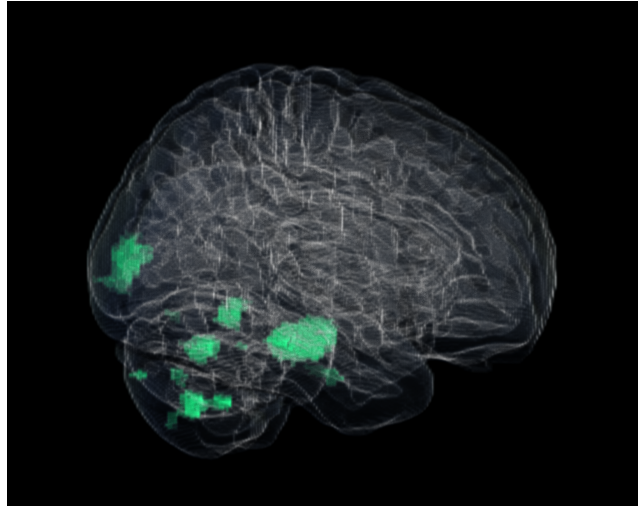


Figure 3. A 3D-rendered human brain from a sample scan in the *ISLES* dataset, with binary stroke lesions overlaid in green. Participants in the *ISLES* challenge are tasked with developing algorithms for segmenting ischemic brain lesions based on multi-modal MRI data. As depicted in the image, these lesions can be multiple, non-overlapping, and distributed across various locations in the brain.

wise metrics obtained through *panoptica*. We evaluate the submissions from team *seals* (rank #1) [12], *nvauto* (rank #2) and *swan* (rank #3). Team *seals* employs an ensemble of *nnU-Nets* [14]; team *nvauto* applies the *Auto3dSeg* pipeline [34] from *MONAI* [7], while the team *swan* utilizes a non-negative matrix factorization neural network [1]. Performance metrics obtained for each of these algorithms are summarized in Table 2.

Submission	Global Metrics		Instance-wise Metrics		
	$gvDSC \uparrow$	$RQ \uparrow$	$SQ \uparrow$	$PQ \uparrow$	$SQASSD \downarrow$
seals [12]	0.781 $\pm$ 0.181	<b>0.52</b> $\pm$ 0.285	<b>0.669</b> $\pm$ 0.217	<b>0.380</b> $\pm$ 0.215	0.312 $\pm$ 0.175
nvauto [34]	<b>0.783</b> $\pm$ 0.177	0.485 $\pm$ 0.278	<b>0.669</b> $\pm$ 0.217	0.357 $\pm$ 0.211	<b>0.307</b> $\pm$ 0.166
swan [1]	0.763 $\pm$ 0.194	0.462 $\pm$ 0.285	0.634 $\pm$ 0.253	0.334 $\pm$ 0.213	0.353 $\pm$ 0.292

Table 2. Performance metrics for the top-three ranked *ISLES’22* challenge algorithms computed with an *IoU* threshold of 0.5 for both matching and evaluation. Besides *gvDSC*, we report instance-wise metrics, cf. Section 4. Mean  $\pm$  standard deviation values are reported. Metrics with  $\uparrow$  are better, the higher the value, while  $\downarrow$  is the opposite. The best values for each metric are highlighted in bold. Statistics for *SQASSD* were performed disregarding infinite values, which involved 13 samples from the teams *seals* and *nvauto* and 19 samples from the team *swan*. Results show that team *nvauto* provided an overall better semantic segmentation performance in terms of *gvDSC*, while the team *seals* achieved better segmentation performance at the instance level.

### 4.3. BraTS Mets experiment

The *BraTS Mets* experiment represents a use case for instance-wise evaluation of semantic segmentation maps. Although metastasis segmentation is an instance segmentation task from a clinical perspective, similar to stroke segmentation cf. Section 4.2, it is typically operationalized as a *SemS* task in *ML*, cf. Section 1.

**Segmentation Task:** The original segmentation task of the *ASNR-MICCAI BraTS Brain Metastasis Challenge (BraTS-M)* [28] is a multi-class hierarchical semantic segmentation task, cf. Figure 4.

**Data:** We evaluate on the publicly available training set of the *BraTS-M* [28]. The dataset consists of 726 examinations, each containing four *MRI* sequences, namely a *pre-contrast T1-weighted (t1w)*, a *post-contrast T1-weighted (t1c)*, a *T2-weighted (t2w)*, and a *T2-weighted Fluid Attenuated Inversion Recovery (t2f)* sequence combined with a multi-class semantic segmentation label, cf. Figure 4. Metastases counts in the dataset hugely vary between 1 and 393 (mean  $8.68 \pm 18.64$ ) per exam.

**Procedure:** To explore how the glioma segmentation algorithms are able to generalize to cancer metastasis segmentation, we conduct the following *off-label use experiment*. We segment the whole dataset with five publicly available glioma *SemS* algorithms distributed through *BraTS Toolkit* [20], namely *hnfnetv1-20* [16], *isen-20* [15], *sanet0-20* [39], *scan-lite-20* [27], and *yixinmpl-20* [38]. Additionally, we derive a sixth segmentation map named *simple* by fusing the five previously obtained algorithms using the implementation of the *SIMPLE* [25] fusion algorithm in *BraTS Toolkit* [20]. We then compute the *gvDSC* and the instance-wise metrics using *panoptica*, cf. Section 4. The results of this analysis are illustrated in Table 3.

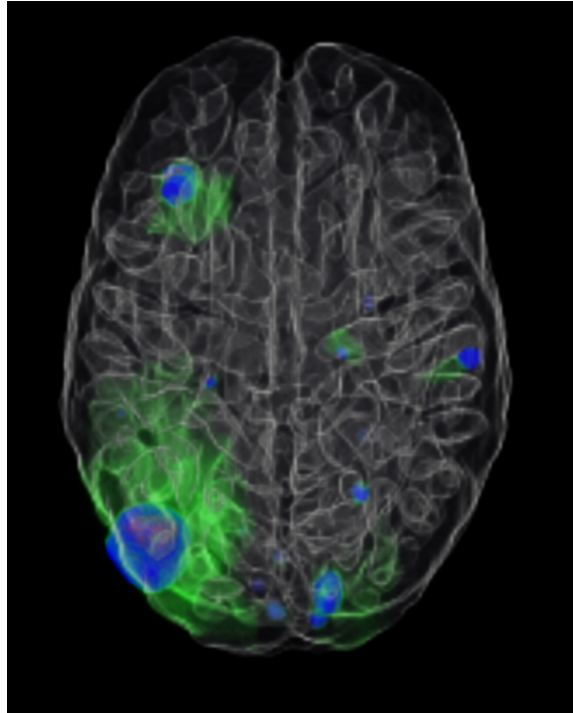


Figure 4. The *BraTS-M* hierarchical semantic segmentation task - axial view of 3D rendered brain with overlaid colored segmentation. The *BraTS-M* [28] segmentation task is inspired by the adult glioma *RSNA-ASNR-MICCAI BraTS Continuous Evaluation Challenge (BraTS-G)* [2]. The glioma lesions are segmented with the classes *Enhancing Tumor (ET)* (blue), *Nonenhancing Tumor Core (NETC)* (red), and *Surrounding Non-enhancing FLAIR Hyperintensity (SNFH)* (green). However, the algorithms are trained and evaluated on hierarchical class channels building upon each other, namely, first, the *enhancing tumor* channel, which consists only of such. Furthermore, the *tumor core* channel combines *ET* and *NETC*, and the *whole tumor* channel combines all three classes. The instance-wise evaluation presented in Table 3 considers only the *tumor core* channel.

Submission	Global Metrics		Instance-wise Metrics		
	$gvDSC \uparrow$	$RQ \uparrow$	$SQ \uparrow$	$PQ \uparrow$	$SQASSD \downarrow$
hnfnetv1-20 [16]	$0.52 \pm 0.39$	$0.33 \pm 0.35$	$0.50 \pm 0.39$	$0.27 \pm 0.28$	$0.65 \pm 0.37$
isen-20 [15]	<b><math>0.54 \pm 0.39</math></b>	<b><math>0.37 \pm 0.36</math></b>	$0.52 \pm 0.38$	<b><math>0.29 \pm 0.30</math></b>	<b><math>0.64 \pm 0.32</math></b>
sanet0-20 [39]	$0.53 \pm 0.38$	$0.35 \pm 0.35$	<b><math>0.53 \pm 0.38</math></b>	$0.28 \pm 0.29$	$0.65 \pm 0.35$
scan_lite-20 [27]	$0.49 \pm 0.37$	$0.32 \pm 0.35$	$0.46 \pm 0.38$	$0.25 \pm 0.28$	$0.70 \pm 0.38$
yixinmpl-20 [38]	$0.52 \pm 0.38$	$0.34 \pm 0.35$	$0.50 \pm 0.37$	$0.27 \pm 0.28$	$0.70 \pm 0.34$
simple [25]	$0.52 \pm 0.39$	$0.35 \pm 0.36$	$0.51 \pm 0.38$	$0.28 \pm 0.29$	$0.68 \pm 0.36$

Table 3. Table summarizing the *BraTS Mets experiment* for an *IOU* threshold of 0.5 for both matching and evaluation. Besides *gvDSC*, we report instance-wise metrics, cf. Section 4. Mean  $\pm$  standard deviation values are reported. Metrics with  $\uparrow$  are better, the higher the value, while  $\downarrow$  is the opposite. The best values for each metric are highlighted in bold. We observe that all algorithms miss many metastases as reflected by the low *RQ*. Further, the *SQ* and *SQASSD* for the correctly detected metastases are only moderate, resulting in an overall low *PQ*. Since *SQASSD* is only a number for patients with matched instances (cf. Section 3.3), samples have been excluded from the calculation of this metric (from 238 for *sanet0-20* up to 286 for *scan\_lite-20*). The low *PQ* and *gvDSC* indicate that the glioma algorithms are not able to generalize well to cancer metastasis segmentation. This is even worse than the moderate *gvDSC* suggests, as indicated by the discrepancy between *PQ* and *gvDSC*.

## 5. Discussion

*panoptica* is an open-source, performance-optimized package written in Python. It allows the computation of instance-wise segmentation quality metrics, for instance- and semantic segmentation maps. Especially in the biomedical domain, for which we demonstrate three example use cases, instance-wise evaluation can be crucial to achieving a better representation of the underlying clinical task. Beyond our examples, there are countless segmentation problems, such as cell counting, that can profit from an instance-wise evaluation. As this also applies to the segmentation of natural images, *panoptica* is not limited to applications in the biomedical domain.

**Limitations and future work:** Transforming semantic segmentation problems into instance segmentation outputs via *CCA* comes with the drawback of typically discarding predicted class scores by relying on integer values as label maps. However, predicted class scores can be important and relevant for the validation. Luckily, instance-wise class scores can be retained from the *SemS* as shown in [31].

The metrics provided by *panoptica* can be easily extended to further metrics such as more selection for overlap- and boundary-based metrics, for example, by including *Centerline Dice Similarity Coefficient (clDice)*, *Normalized Surface Dice (NSD)*, or *Hausdorff Distance (HD)*. In addition, the package could be extended to include multi-threshold metrics [26] such as *Average Precision (AP)* and [9] to assess detection quality in more detail. With a more comprehensive list of metrics, the package will be able to offer a more extensive performance assessment from different viewpoints and allow users to select the most suitable choices for their application.

The current package implements several overlap-based strategies. Another worthy addition would be to implement more matching strategies to cover a bigger variety of use cases. For example, if predicted class scores are available for each instance, the *Greedy by Score* matching [11] could be applied. This strategy orders predicted instances by their predicted class scores and identifies the matching *reference instance* by choosing the *reference instance* with the highest *Matching Score (MS)*. Next, the *assigned reference instance* will be removed, such that this instance matcher remains a one-to-one matcher. If class scores are not available, the strategy can be simplified to the *Greedy by Localization Criterion* matching [26], which orders predicted instances by the *MS*. Furthermore, more advanced instance matchers like the *Optimal Hungarian Matching* [24] can be applied, which minimizes a cost function dependent on the *Matching Metric (MM)*. Another interesting idea would be to implement matching based on topological features.

Similarly, we aim to extend the type of *MM* to include all localization criteria mentioned in the *Metrics Reloaded* framework [26], as it has been shown [26] that *IOU* is not always the best option for a localization criterion. For a comprehensive analysis of performance variability, we aim to expand the notion of mean and standard deviation to confidence intervals, for example, constructed via bootstrapping.



## References

- [1] Pooya Ashtari, Diana M Sima, Lieven De Lathauwer, Dominique Sappey-Mariniere, Frederik Maes, and Sabine Van Huffel. Factorizer: A scalable interpretable approach to context modeling for medical image segmentation. *Medical image analysis*, 84:102706, 2023. 6, 7
- [2] Spyridon Bakas, Mauricio Reyes, Andras Jakab, Stefan Bauer, Markus Rempfler, Alessandro Crimi, Russell Takeshi Shinohara, Christoph Berger, Sung Min Ha, Martin Rozycki, Marcel Prastawa, Esther Alberts, Jana Lipkova, John Freymann, Justin Kirby, Michel Bilello, Hassan Fathallah-Shaykh, Roland Wiest, Jan Kirschke, Benedikt Wiestler, Rivka Colen, Aikaterini Kotrotsou, Pamela Lamontagne, Daniel Marcus, Mikhail Milchenko, Arash Nazeri, Marc-Andre Weber, Abhishek Mahajan, Ujjwal Baid, Elizabeth Gerstner, Dongjin Kwon, Gagan Acharya, Manu Agarwal, Mahbulul Alam, Alberto Albiol, Antonio Albiol, Francisco J. Albiol, Varghese Alex, Nigel Allinson, Pedro H. A. Amorim, Abhijit Amrutkar, Ganesh Anand, Simon Andermatt, Tal Arbel, Pablo Arbelaez, Aaron Avery, Muneeza Azmat, Pranjal B., W Bai, Subhashis Banerjee, Bill Barth, Thomas Batchelder, Kayhan Batmanghelich, Enzo Battistella, Andrew Beers, Mikhail Belyaev, Martin Bendszus, Eze Benson, Jose Bernal, Halandur Nagaraja Bharath, George Biros, Sotirios Bisdas, James Brown, Mariano Cabezas, Shilei Cao, Jorge M. Cardoso, Eric N Carver, Adrià Casamitjana, Laura Silvana Castillo, Marcel Catà, Philippe Cattin, Albert Cerigues, Vinicius S. Chagas, Siddhartha Chandra, Yi-Ju Chang, Shiyu Chang, Ken Chang, Joseph Chazalon, Shengcong Chen, Wei Chen, Jefferson W Chen, Zhaolin Chen, Kun Cheng, Ahana Roy Choudhury, Roger Chylla, Albert Clérigues, Steven Coleman, Ramiro German Rodriguez Colmeiro, Marc Combalia, Anthony Costa, Xiaomeng Cui, Zhenzhen Dai, Lutao Dai, Laura Alexandra Daza, Eric Deutsch, Changxing Ding, Chao Dong, Shidu Dong, Wojciech Dudzik, Zach Eaton-Rosen, Gary Egan, Guilherme Escudero, Théo Estienne, Richard Everson, Jonathan Fabrizio, Yong Fan, Longwei Fang, Xue Feng, Enzo Ferrante, Lucas Fidon, Martin Fischer, Andrew P. French, Naomi Fridman, Huan Fu, David Fuentes, Yaozong Gao, Evan Gates, David Gering, Amir Gholami, Willi Gierke, Ben Glocker, Mingming Gong, Sandra González-Villá, T. Groszges, Yuanfang Guan, Sheng Guo, Sudeep Gupta, Woo-Sup Han, Il Song Han, Konstantin Harmuth, Huiguang He, Aura Hernández-Sabaté, Evelyn Herrmann, Naveen Himthani, Winston Hsu, Cheyu Hsu, Xiaojun Hu, Xiaobin Hu, Yan Hu, Yifan Hu, Rui Hua, Teng-Yi Huang, Weilin Huang, Sabine Van Huffel, Quan Huo, Vivek HV, Khan M. Iftekharruddin, Fabian Isensee, Mobarakol Islam, Aaron S. Jackson, Sachin R. Jambawalikar, Andrew Jesson, Weijian Jian, Peter Jin, V Jeya Maria Jose, Alain Jungo, B Kainz, Konstantinos Kamnitsas, Po-Yu Kao, Ayush Karnawat, Thomas Kellermeier, Adel Kermi, Kurt Keutzer, Mohamed Tarek Khadir, Mahendra Khened, Philipp Kickingereder, Geena Kim, Nik King, Haley Knapp, Urspeter Knecht, Lisa Kohli, Deren Kong, Xiangmao Kong, Simon Koppers, Avinash Kori, Ganapathy Krishnamurthi, Egor Krivov, Piyush Kumar, Kaiser Kushibar, Dmitrii Lachinov, Tryphon Lambrou, Joon Lee, Chengen Lee, Yuehchou Lee, M Lee, Szidonia Lefkovits, Laszlo Lefkovits, James Levitt, Tengfei Li, Hongwei Li, Wenqi Li, Hongyang Li, Xiaochuan Li, Yuexiang Li, Heng Li, Zhenye Li, Xiaoyu Li, Zeju Li, XiaoGang Li, Wenqi Li, Zheng-Shen Lin, Fengming Lin, Pietro Lio, Chang Liu, Boqiang Liu, Xiang Liu, Mingyuan Liu, Ju Liu, Luyan Liu, Xavier Llado, Marc Moreno Lopez, Pablo Ribalta Lorenzo, Zhentai Lu, Lin Luo, Zhigang Luo, Jun Ma, Kai Ma, Thomas Mackie, Anant Madabushi, Issam Mahmoudi, Klaus H. Maier-Hein, Pradipta Maji, CP Mammen, Andreas Mang, B. S. Manjunath, Michal Marcinkiewicz, S McDonagh, Stephen McKenna, Richard McKinley, Miriam Mehl, Sachin Mehta, Raghav Mehta, Raphael Meier, Christoph Meinel, Dorit Merhof, Craig Meyer, Robert Miller, Sushmita Mitra, Aliasgar Moiyadi, David Molina-Garcia, Miguel A. B. Monteiro, Grzegorz Mrukwa, Andriy Myronenko, Jakub Nalepa, Thuyen Ngo, Dong Nie, Holly Ning, Chen Niu, Nicholas K Nuechterlein, Eric Oermann, Arlindo Oliveira, Diego D. C. Oliveira, Arnau Oliver, Alexander F. I. Osman, Yu-Nian Ou, Sebastian Ourselin, Nikos Paragios, Moo Sung Park, Brad Paschke, J. Gregory Pauloski, Kamlesh Pawar, Nick Pawlowski, Linmin Pei, Suting Peng, Silvio M. Pereira, Julian Perez-Beteta, Victor M. Perez-Garcia, Simon Pezold, Bao Pham, Ashish Phophalia, Gemma Piella, G. N. Pillai, Marie Piraud, Maxim Pisov, Anmol Popli, Michael P. Pound, Reza Pourreza, Prateek Prasanna, Vesna Prkowska, Tony P. Pridmore, Santi Puch, Élodie Puybareau, Buyue Qian, Xu Qiao, Martin Rajchl, Swapnil Rane, Michael Rebsamen, Hongliang Ren, Xuhua Ren, Karthik Revanuru, Mina Rezaei, Oliver Rippel, Luis Carlos Rivera, Charlotte Robert, Bruce Rosen, Daniel Rueckert, Mohammed Safwan, Mostafa Salem, Joaquim Salvi, Irina Sanchez, Irina Sánchez, Heitor M. Santos, Emmett Sartor, Dawid Schellingerhout, Klaudius Scheufele, Matthew R. Scott, Artur A. Scussel, Sara Sedlar, Juan Pablo Serrano-Rubio, N. Jon Shah, Nameetha Shah, Mazhar Shaikh, B. Uma Shankar, Zeina Shboul, Haipeng Shen, Dinggang Shen, Linlin Shen, Haocheng Shen, Varun Shenoy, Feng Shi, Hyung Eun Shin, Hai Shu, Diana Sima, M Sinclair, Orjan Smedby, James M. Snyder, Mohammadreza Soltaninejad, Guidong Song, Mehul Soni, Jean Stawiaski, Shashank Subramanian, Li Sun, Roger Sun, Jiawei Sun, Kay Sun, Yu Sun, Guoxia Sun, Shuang Sun, Yannick R Suter, Laszlo Szilagyi, Sanjay Talbar, Dacheng Tao, Dacheng Tao, Zhongzhao Teng, Siddhesh Thakur, Meenakshi H Thakur, Sameer Tharakan, Pallavi Tiwari, Guillaume Tochon, Tuan Tran, Yuhsiang M. Tsai, Kuan-Lun Tseng, Tran Anh Tuan, Vadim Turlapov, Nicholas Tustison, Maria Vakalopoulou, Sergi Valverde, Rami Vanguri, Evgeny Vasiliev, Jonathan Ventura, Luis Vera, Tom Vercauteren, C. A. Verrastro, Lasitha Vidyaratne, Veronica Vilaplana, Ajeet Vivekanandan, Guotai Wang, Qian Wang, Chiatse J. Wang, Weichung Wang, Duo Wang, Ruixuan Wang, Yuanyuan Wang, Chunliang Wang, Guotai Wang, Ning Wen, Xin Wen, Leon Weninger, Wolfgang Wick, Shaocheng Wu, Qiang Wu, Yihong Wu, Yong Xia, Yanwu Xu, Xiaowen Xu, Peiyuan Xu, Tsai-Ling Yang, Xiaoping Yang, Hao-Yu Yang, Junlin Yang, Haojin

- Yang, Guang Yang, Hongdou Yao, Xujiang Ye, Changchang Yin, Brett Young-Moxon, Jinhua Yu, Xiangyu Yue, Songtao Zhang, Angela Zhang, Kun Zhang, Xuejie Zhang, Lichi Zhang, Xiaoyue Zhang, Yazhuo Zhang, Lei Zhang, Jianguo Zhang, Xiang Zhang, Tianhao Zhang, Sicheng Zhao, Yu Zhao, Xiaomei Zhao, Liang Zhao, Yefeng Zheng, Liming Zhong, Chenhong Zhou, Xiaobing Zhou, Fan Zhou, Hongtu Zhu, Jin Zhu, Ying Zhuge, Weiwei Zong, Jayashree Kalpathy-Cramer, Keyvan Farahani, Christos Davatzikos, Koen van Leemput, and Bjoern Menze. Identifying the best machine learning algorithms for brain tumor segmentation, progression assessment, and overall survival prediction in the brats challenge, 2019. [2](#), [4](#), [7](#)
- [3] Harsharan Singh Bhatia, Andreas-David Brunner, Furkan Öztürk, Saketh Kapoor, Zhouyi Rong, Hongcheng Mai, Marvin Thielert, Mayar Ali, Rami Al-Maskari, Johannes Christian Paetzold, et al. Spatial proteomics in three-dimensional intact specimens. *Cell*, 185(26):5040–5058, 2022. [2](#)
- [4] Patrick Bilic, Patrick Christ, Hongwei Bran Li, Eugene Vorontsov, Avi Ben-Cohen, Georgios Kaissis, Adi Szeskin, Colin Jacobs, Gabriel Efrain Humpire Mamani, Gabriel Chartrand, et al. The liver tumor segmentation benchmark (lits). *Medical Image Analysis*, 84:102680, 2023. [2](#)
- [5] Josef A Buchner, Florian Kofler, Lucas Etzel, Michael Mayinger, Sebastian M Christ, Thomas B Brunner, Andrea Wittig, Björn Menze, Claus Zimmer, Bernhard Meyer, et al. Development and external validation of an mri-based neural network for brain metastasis segmentation in the aurora multicenter study. *Radiotherapy and Oncology*, 178:109425, 2023. [2](#)
- [6] Josef A Buchner, Jan C Peeken, Lucas Etzel, Ivan Ezhov, Michael Mayinger, Sebastian M Christ, Thomas B Brunner, Andrea Wittig, Bjoern H Menze, Claus Zimmer, et al. Identifying core mri sequences for reliable automatic brain metastasis segmentation. *Radiotherapy and Oncology*, 188:109901, 2023. [2](#)
- [7] M Jorge Cardoso, Wenqi Li, Richard Brown, Nic Ma, Eric Kerfoot, Yiheng Wang, Benjamin Murrey, Andriy Myronenko, Can Zhao, Dong Yang, et al. Monai: An open-source framework for deep learning in healthcare. *arXiv preprint arXiv:2211.02701*, 2022. [2](#), [6](#)
- [8] Hao Chen, Chiyao Shen, Jing Qin, Dong Ni, Lin Shi, Jack C. Y. Cheng, and Pheng-Ann Heng. Automatic localization and identification of vertebrae in spine ct via a joint learning model with deep neural networks. In *Medical Image Computing and Computer-Assisted Intervention – MICCAI 2015*, pages 515–522, Cham, 2015. Springer International Publishing. [6](#)
- [9] Long Chen, Yuli Wu, Johannes Stegmaier, and Dorit Merhof. Sortedap: Rethinking evaluation metrics for instance segmentation. In *Proceedings of the IEEE/CVF International Conference on Computer Vision*, pages 3923–3929, 2023. [2](#), [8](#)
- [10] Nicki Skaftø Detlefsen, Jiri Borovec, Justus Schock, Ananya Harsh Jha, Teddy Koker, Luca Di Liello, Daniel Stancl, Changsheng Quan, Maxim Grechkin, and William Falcon. Torchmetrics-measuring reproducibility in pytorch. *Journal of Open Source Software*, 7(70):4101, 2022. [2](#)
- [11] Mark Everingham, SM Ali Eslami, Luc Van Gool, Christopher KI Williams, John Winn, and Andrew Zisserman. The pascal visual object classes challenge: A retrospective. *International journal of computer vision*, 111(1):98–136, 2015. [8](#)
- [12] Shengbo Gao. SEALS- ISLES’22 participating method. [https://github.com/Tabrisrei/ISLES22\\_SEALS](https://github.com/Tabrisrei/ISLES22_SEALS), 2022. [Online; accessed 16-November-2023]. [6](#), [7](#)
- [13] Moritz R Hernandez Petzsche, Ezequiel de la Rosa, Uta Hanning, Roland Wiest, Waldo Valenzuela, Mauricio Reyes, Maria Meyer, Sook-Lei Liew, Florian Kofler, Ivan Ezhov, et al. Isles 2022: A multi-center magnetic resonance imaging stroke lesion segmentation dataset. *Scientific data*, 9(1):762, 2022. [2](#), [6](#)
- [14] Fabian Isensee, Paul F Jaeger, Simon AA Kohl, Jens Petersen, and Klaus H Maier-Hein. nnu-net: a self-configuring method for deep learning-based biomedical image segmentation. *Nature methods*, 18(2):203–211, 2021. [2](#), [6](#)
- [15] Fabian Isensee, Paul F Jäger, Peter M Full, Philipp Vollmuth, and Klaus H Maier-Hein. nnu-net for brain tumor segmentation. In *Brainlesion: Glioma, Multiple Sclerosis, Stroke and Traumatic Brain Injuries: 6th International Workshop, BrainLes 2020, Held in Conjunction with MICCAI 2020, Lima, Peru, October 4, 2020, Revised Selected Papers, Part II 6*, pages 118–132. Springer, 2021. [7](#), [8](#)
- [16] Haozhe Jia, Weidong Cai, Heng Huang, and Yong Xia. H<sup>2</sup> 2 nf-net for brain tumor segmentation using multimodal mr imaging: 2nd place solution to brats challenge 2020 segmentation task. In *Brainlesion: Glioma, Multiple Sclerosis, Stroke and Traumatic Brain Injuries: 6th International Workshop, BrainLes 2020, Held in Conjunction with MICCAI 2020, Lima, Peru, October 4, 2020, Revised Selected Papers, Part II 6*, pages 58–68. Springer, 2021. [7](#), [8](#)
- [17] Alain Jungo, Olivier Scheidegger, Mauricio Reyes, and Fabian Balsiger. pymia: A python package for data handling and evaluation in deep learning-based medical image analysis. *Computer methods and programs in biomedicine*, 198:105796, 2021. [2](#)
- [18] Doris Kaltenecker, Rami Al-Maskari, Moritz Negwer, Luciano Hoehner, Florian Kofler, Shan Zhao, Mihail Todorov Todorov, Johannes Christian Paetzold, Benedikt Wiestler, Julia Geppert, et al. Virtual reality empowered deep learning analysis of brain activity. *bioRxiv*, pages 2023–05, 2023. [2](#)
- [19] Alexander Kirillov, Kaiming He, Ross Girshick, Carsten Rother, and Piotr Dollár. Panoptic segmentation. In *Proceedings of the IEEE/CVF conference on computer vision and pattern recognition*, pages 9404–9413, 2019. [1](#), [2](#), [4](#)
- [20] Florian Kofler, Christoph Berger, Diana Waldmannstetter, Jana Lipkova, Ivan Ezhov, Giles Tetteh, Jan Kirschke, Claus Zimmer, Benedikt Wiestler, and Bjoern H Menze. Brats toolkit: translating brats brain tumor segmentation algorithms into clinical and scientific practice. *Frontiers in neuroscience*, page 125, 2020. [2](#), [7](#)
- [21] Florian Kofler, Ivan Ezhov, Fabian Isensee, Fabian Balsiger, Christoph Berger, Maximilian Koerner, Johannes Paetzold,

- Hongwei Li, Suprosanna Shit, Richard McKinley, et al. Are we using appropriate segmentation metrics? identifying correlates of human expert perception for cnn training beyond rolling the dice coefficient. [arXiv preprint arXiv:2103.06205](#), 2021. [2](#)
- [22] Florian Kofler, Suprosanna Shit, Ivan Ezhov, Lucas Fidon, Izabela Horvath, Rami Al-Maskari, Hongwei Bran Li, Harsharan Bhatia, Timo Loehr, Marie Piraud, et al. blob loss: instance imbalance aware loss functions for semantic segmentation. In [International Conference on Information Processing in Medical Imaging](#), pages 755–767. Springer Nature Switzerland Cham, 2023. [2](#)
- [23] Florian Kofler, Johannes Wahle, Ivan Ezhov, Sophia J Wagner, Rami Al-Maskari, Emilia Gryska, Mihail Todorov, Christina Bukas, Felix Meissen, Tingying Peng, et al. Approaching peak ground truth. In [2023 IEEE 20th International Symposium on Biomedical Imaging \(ISBI\)](#), pages 1–6. IEEE, 2023. [4](#)
- [24] Harold W Kuhn. The hungarian method for the assignment problem. [Naval research logistics quarterly](#), 2(1-2):83–97, 1955. [8](#)
- [25] Thomas Robin Langerak, Uulke A van der Heide, Alexis NTJ Kotte, Max A Viergever, Marco Van Vulpen, and Josien PW Pluim. Label fusion in atlas-based segmentation using a selective and iterative method for performance level estimation (simple). [IEEE transactions on medical imaging](#), 29(12):2000–2008, 2010. [7](#), [8](#)
- [26] Lena Maier-Hein, Annika Reinke, Patrick Godau, Minu D. Tizabi, Florian Buettner, Evangelia Christodoulou, Ben Glocker, Fabian Isensee, Jens Kleesiek, Michal Kozubek, Mauricio Reyes, Michael A. Riegler, Manuel Wiesenfarth, A. Emre Kavur, Carole H. Sudre, Michael Baumgartner, Matthias Eisenmann, Doreen Heckmann-Nötzel, A. Tim Rädtsch, Laura Acion, Michela Antonelli, Tal Arbel, Spyridon Bakas, Arriel Benis, Matthew Blaschko, M. Jorge Cardoso, Veronika Cheplygina, Beth A. Cimini, Gary S. Collins, Keyvan Farahani, Luciana Ferrer, Adrian Galdran, Bram van Ginneken, Robert Haase, Daniel A. Hashimoto, Michael M. Hoffman, Merel Huisman, Pierre Jannin, Charles E. Kahn, Dagmar Kainmueller, Bernhard Kainz, Alexandros Karargyris, Alan Karthikesalingam, Hannes Kenngott, Florian Kofler, Annette Kopp-Schneider, Anna Kreshuk, Tahsin Kurc, Bennett A. Landman, Geert Litjens, Amin Madani, Klaus Maier-Hein, Anne L. Martel, Peter Mattson, Erik Meijering, Bjoern Menze, Karel G. M. Moons, Henning Müller, Brennan Nichyporuk, Felix Nickel, Jens Petersen, Nasir Rajpoot, Nicola Rieke, Julio Saez-Rodriguez, Clara I. Sánchez, Shravya Shetty, Maarten van Smeden, Ronald M. Summers, Abdel A. Taha, Aleksei Tiulpin, Sotirios A. Tsaftaris, Ben Van Calster, Gaël Varoquaux, and Paul F. Jäger. Metrics reloaded: Recommendations for image analysis validation, 2023. [2](#), [8](#)
- [27] Richard McKinley, Micheal Rebsamen, Katrin Dätwyler, Raphael Meier, Piotr Radojewski, and Roland Wiest. Uncertainty-driven refinement of tumor-core segmentation using 3d-to-2d networks with label uncertainty. In [Brainlesion: Glioma, Multiple Sclerosis, Stroke and Traumatic Brain Injuries: 6th International Workshop, BrainLes 2020, Held in Conjunction with MICCAI 2020, Lima, Peru, October 4, 2020, Revised Selected Papers, Part I 6](#), pages 401–411. Springer, 2021. [7](#), [8](#)
- [28] Ahmed W Moawad, Anastasia Janas, Ujjwal Baid, Divya Ramakrishnan, Leon Jekel, Kiril Krantchev, Harrison Moy, Rachit Saluja, Klara Osenberg, Klara Wilms, et al. The brain tumor segmentation (brats-mets) challenge 2023: Brain metastasis segmentation on pre-treatment mri. [ArXiv](#), 2023. [7](#)
- [29] Christian Payer., Darko Štern., Horst Bischof., and Martin Urschler. Coarse to fine vertebrae localization and segmentation with spatialconfiguration-net and u-net. In [Proceedings of the 15th International Joint Conference on Computer Vision, Imaging and Computer Graphics Theory and Applications \(VISIGRAPP 2020\) - Volume 5: VISAPP](#), pages 124–133. INSTICC, SciTePress, 2020. [6](#)
- [30] Chinmay Prabhakar, Hongwei Bran Li, Johannes C Paetzold, Timo Loehr, Chen Niu, Mark Mühlau, Daniel Rueckert, Benedikt Wiestler, and Bjoern Menze. Self-pruning graph neural network for predicting inflammatory disease activity in multiple sclerosis from brain mr images. In [International Conference on Medical Image Computing and Computer-Assisted Intervention](#), pages 226–236. Springer, 2023. [1](#)
- [31] Annika Reinke, Minu D Tizabi, Carole H Sudre, Matthias Eisenmann, Tim Rädtsch, Michael Baumgartner, Laura Acion, Michela Antonelli, Tal Arbel, Spyridon Bakas, et al. Common limitations of image processing metrics: A picture story. [arXiv preprint arXiv:2104.05642](#), 2021. [2](#), [8](#)
- [32] Olaf Ronneberger, Philipp Fischer, and Thomas Brox. U-net: Convolutional networks for biomedical image segmentation. In [Medical Image Computing and Computer-Assisted Intervention – MICCAI 2015](#), pages 234–241, Cham, 2015. Springer International Publishing. [2](#)
- [33] Anjany Sekuboyina, Malek E Hussein, Amirhossein Bayat, Maximilian Löffler, Hans Liebl, Hongwei Li, Giles Tetteh, Jan Kukačka, Christian Payer, Darko Štern, et al. Verse: a vertebrae labelling and segmentation benchmark for multi-detector ct images. [Medical image analysis](#), 73:102166, 2021. [2](#), [5](#), [6](#)
- [34] Md Mahfuzur Rahman Siddique, Dong Yang, Yufan He, Daguang Xu, and Andriy Myronenko. Automated ischemic stroke lesion segmentation from 3d mri. [arXiv preprint arXiv:2209.09546](#), 2022. [6](#), [7](#)
- [35] William Silversmith. cc3d: Connected components on multilabel 3D & 2D images. [Zenodo](#), 2021. [3](#)
- [36] Carole H Sudre, Kimberlin Van Wijnen, Florian Dubost, Hieab Adams, David Atkinson, Frederik Barkhof, Mahlet A Birhanu, Esther E Bron, Robin Camarasa, Nish Chaturvedi, et al. Where is valdo? vascular lesions detection and segmentation challenge at miccai 2021. [arXiv preprint arXiv:2208.07167](#), 2022. [2](#)
- [37] Alan J Thompson, Brenda L Banwell, Frederik Barkhof, William M Carroll, Timothy Coetzee, Giancarlo Comi, Jorge Correale, Franz Fazekas, Massimo Filippi, Mark S Freedman, et al. Diagnosis of multiple sclerosis: 2017 revisions of the mcdonald criteria. [The Lancet Neurology](#), 17(2):162–173, 2018. [2](#)

- [38] Yixin Wang, Yao Zhang, Feng Hou, Yang Liu, Jiang Tian, Cheng Zhong, Yang Zhang, and Zhiqiang He. Modality-pairing learning for brain tumor segmentation. In Brainlesion: Glioma, Multiple Sclerosis, Stroke and Traumatic Brain Injuries: 6th International Workshop, BrainLes 2020, Held in Conjunction with MICCAI 2020, Lima, Peru, October 4, 2020, Revised Selected Papers, Part I 6, pages 230–240. Springer, 2021. [7](#), [8](#)
- [39] Yading Yuan. Automatic brain tumor segmentation with scale attention network. In Brainlesion: Glioma, Multiple Sclerosis, Stroke and Traumatic Brain Injuries: 6th International Workshop, BrainLes 2020, Held in Conjunction with MICCAI 2020, Lima, Peru, October 4, 2020, Revised Selected Papers, Part I 6, pages 285–294. Springer, 2021. [7](#), [8](#)

## 42. Supplemental Material

### 42.1. CCA Benchmark: *cc3d* vs. *scipy*

Table 4 summarizes the comparison of CCA backends. The code for the comparison is [publicly available](#).

Dimensionality	Volume Size	Scipy Time [s]	CC3D Time [s]
2D	500 <sup>2</sup>	<b>0.0350</b>	0.0552
	1000 <sup>2</sup>	<b>0.1344</b>	0.2268
	2000 <sup>2</sup>	<b>0.5121</b>	0.8542
	4000 <sup>2</sup>	<b>2.1542</b>	3.4198
	8000 <sup>2</sup>	<b>9.5657</b>	16.4068
3D	50 <sup>3</sup>	0.0204	<b>0.0144</b>
	100 <sup>3</sup>	0.1564	<b>0.1160</b>
	200 <sup>3</sup>	1.2277	<b>0.9043</b>
	500 <sup>3</sup>	20.7657	<b>15.3032</b>
	1000 <sup>3</sup>	195.1927	<b>145.1652</b>

Table 4. Benchmarking Scipy’s *skimage* vs. *cc3d* for connected component analysis for random binary 2D and 3D data. The benchmark suggests that *Skimage* is more efficient for 2D data, while *cc3d* performs better for 3D data. The tests were conducted on an Apple M1 Pro Processor. *panoptica* comes with [code](#) to benchmark which backend performs better on the given hardware.

### 42.2. Computation times

We benchmark the three modules from *panoptica* on exemplary samples. Across all these performance tests, we use instance approximation based on CCA, instance matching with the naive one-to-one setting (cf. Section 3.2) using *IOU* as *MM*, and evaluate the instance-wise metrics *RQ*, *SQ*, *PQ* and *ASSD*. For all experiments, we use a *IOU* threshold of 0.5 both for matching and evaluation. The following test setups are used:

- Work station: Ubuntu 22.04, AMD Ryzen 9 5900x, 128GB RAM
- Apple Macbook Pro with M1 Max 10-Core processor, 32GB RAM

The code to run the benchmark is [publicly available](#). The exemplary samples include:

- 2d\_simple: A simulated (50,50) 2D input consisting of two instances both in prediction and reference.
- 3d\_spine: A real MRI spine segmentation sample of shape (170, 512, 17) consisting of 89 prediction instances and 87 reference instances. 73 instances are successfully matched.
- 3d\_dense: A (100, 100, 100) shaped image densely filled with 40 simulated instances both in prediction and reference.

Figure 5 shows the result of our tests.

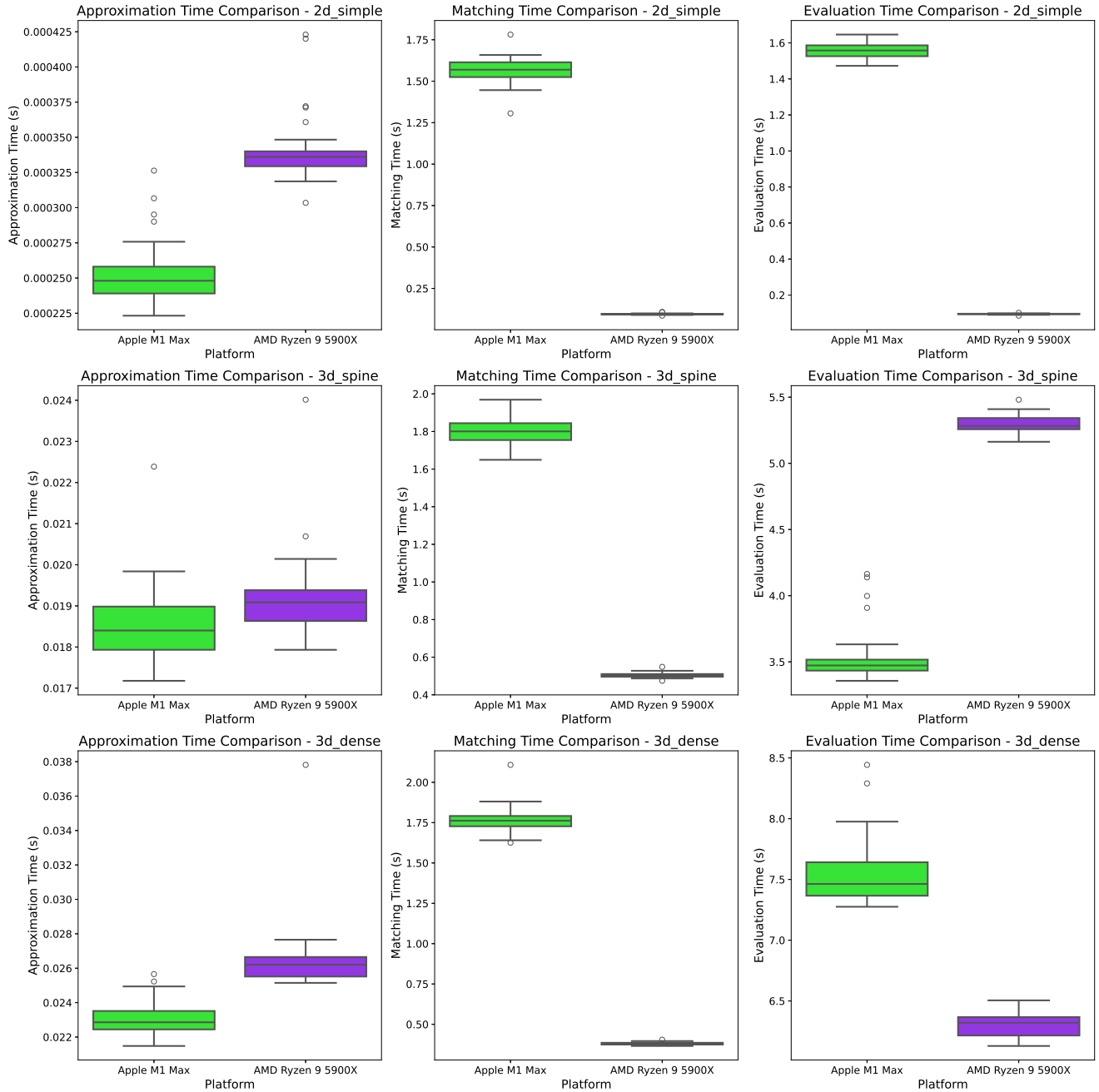


Figure 5. Performance test of the *panoptica* package over two different machines (green and purple) and three unique input samples (rows). Each test shows the mean and standard deviations across 42 iterations for each of the three modules (columns). All measurements are given in seconds. While instance approximation is consistently fast, instance matching and evaluation can take a couple of seconds, depending on the input sizes and parallel processing power of the utilized CPU. As *panoptica* allows the user to specify which metrics should be calculated, these times can vary.

### 42.3. Segmentation Performance over varying IOU-thresholds

With *panoptica* performance measures can easily be computed for various IOU-thresholds, cf. Figure 6. Note that different thresholds could be selected for *instance matching* and *instance evaluation*.

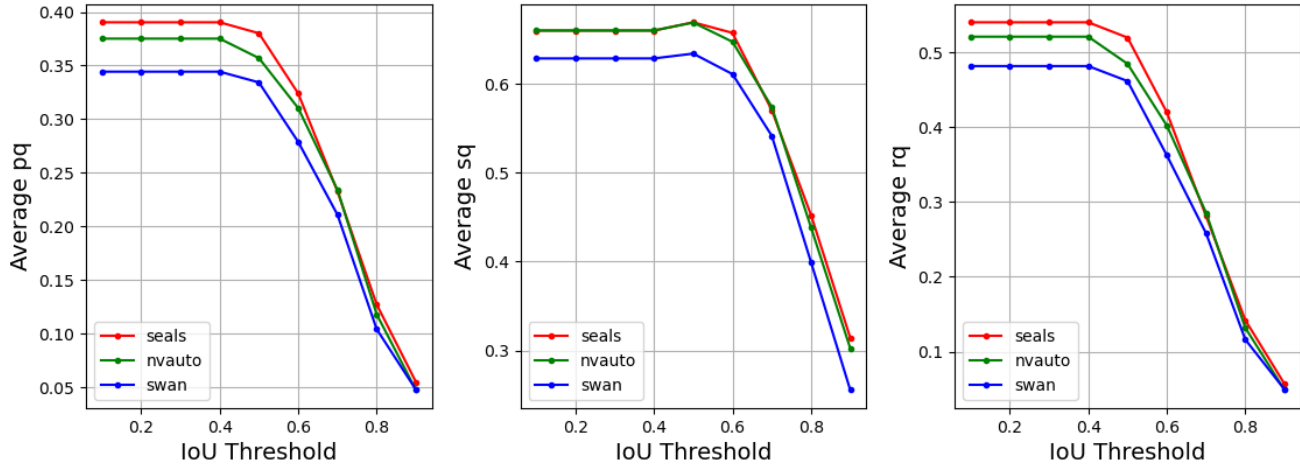


Figure 6. Average  $PQ$  (left),  $-SQ$  (middle),  $-RQ$  (right) for varying IOU-thresholds. Here, the same threshold is applied for both *instance matching* and *instance evaluation*. Each curve represents one of the leading teams of the *ISLES* challenge, cf. Section 4.2. Notably, depending on the IOU threshold and employed metric, it varies which is the optimal algorithm for stroke segmentation. One could consider utilizing the *Area Under the Curve (AUC)* for each algorithm across the entire range of thresholds to provide a holistic performance summary robust to variations in threshold selection.

### Acknowledgement

Bjoern Menze, Benedikt Wiestler, and Florian Kofler are supported through the SFB 824, subproject B12. Supported by Deutsche Forschungsgemeinschaft (DFG) through TUM International Graduate School of Science and Engineering (IGSSE), GSC 81. Supported by Anna Valentina Lioba Eleonora Claire Javid Mamasani. Bjoern Menze acknowledges support by the Helmut Horten Foundation. Ivan Ezhov is supported by the Translational Brain Imaging Training Network (TRABIT) under the European Union’s ‘Horizon 2020’ research & innovation program (Grant agreement ID: 765148). Fabian Isensee is supported by Helmholtz Imaging (HI), a platform of the Helmholtz Incubator on Information and Data Science. Jan Kirschke has received Grants from the ERC, DFG, BMBF and is a Co-Founder of Bonescreen GmbH. Benedikt Wiestler is supported by the NIH (R01CA269948).